Structural Engineering and Mechanics, *Vol. 48, No. 1 (2013) 41-56*
DOI: http://dx.doi.org/10.12989/sem.2013.48.1.041

Prediction of through the width delamination growth in post-buckled laminates under fatigue loading using de-cohesive law

Hossein Hosseini-Toudeshky*[1], M. Saeed Goodarzi[1] and Bijan Mohammadi[2]

[1]*Department of Aerospace Engineering, Amirkabir University of Technology, No. 424, Hafez Ave, Tehran, Iran*
[2]*School of Mechanical Engineering, Iran University of Science and Technology, Tehran, Iran*

(Received June 17, 2013, Revised August 29, 2013, Accepted September 18, 2013)

Abstract. Initiation and growth of delamination is a great concern of designers of composite structures. Interface elements with de-cohesive constitutive law in the content of continuum damage mechanics can be used to predict initiation and growth of delamination in single and mixed mode conditions. In this paper, an interface element based on the cohesive zone method has been developed to simulate delaminatoin growth of post-buckled laminate under fatigue loading. The model was programmed as the user element and user material by the "User Programmable Features" in ANSYS finite element software. The interface element is a three-dimensional 20 node brick with small thickness. Because of mixed-mode condition of stress field at the delamination-front of post-buckled laminates, a mixed-mode bilinear constitutive law has been used as user material in this model. The constitutive law of interface element has been verified by modelling of a single element. A composite laminate with initial delamination under quasi-static compressive Loading available from literature has been remodeled with the present approach. Moreover, it will be shown that, the closer the delamination to the free surface of laminate, the slower the delamination growth under compressive fatigue loading. The effects of laminate configuration on delamination growth are also investigated.

Keywords: interface element; buckling; laminated composites; fatigue; finite element method

1. Introduction

Composite laminates are attractive for many researchers and designers due to their valuable material properties. However, different mechanical behavior of various layers at an interface can cause unwanted damage such as delamination at the manufacturing level or during the service. Several numerical methods have been developed to predict the delamination initiation and growth in composite laminates using finite element method.

Methods based on fracture mechanics approach are useful for the prediction of delamination growth of an initial interface debonding. Methods such as virtual crack closure technique (VCCT) (Rybicki and Kanninen 1977, Krueger 2002) have been widely used to estimate the energy release rate at delamination front. In these methods, Delamination growth is defined when the calculated

*Corresponding author, Professor, E-mail: Hosseini@aut.ac.ir

http://www.techno-press.org/?journal=sem&subpage=8 ISSN: 1225-4568 (Print), 1598-6217 (Online)

energy release rate becomes equal to a critical value (Griffith 1921). Hosseini-Toudeshky *et al*. (2010a) used VCCT method to simulate the growth of small initially observed delamination near the free edges of laminate under quasi-static tensile loading. The drawbacks of these methods are that an initial crack should exist in the model and the entire model should be re-meshed at each crack growth step.

On the other hand, continuum damage mechanic (CDM) approaches are capable to predict the initiation and growth of delamination. Cohesive zone modeling is a powerful method to consider the material nonlinearity of bonded interfaces in both quasi-static and fatigue loading. (Camanho and Davila 2002) developed a cohesive zone model with bilinear constitutive law in order to model the delamination growth in mixed-mode bending specimen. In this model, softening law of cohesive zone was controlled by a displacement based damage parameter. Turon *et al*. (2007a) developed this model to predict delamination growth under high cycle fatigue tensile loadings. Hosseini-Toudeshky *et al*. (2011) also proposed a finite element model to simulate the fatigue progressive debonding of interface between composite patch and cracked aluminum panels concurrent with the crack growth in the base panel. It is worth to note that small deformation theory was employed for the above mention models.

Cyclic loading causes fatigue growth of initiated delaminations. Large displacement and bending due to the post-buckling under compressive loading produces the mixed mode state of stress at delamination front. Kardomateas *et al*. (1995) performed experimental study of delamination growth in unidirectional laminate with pre-existing delamination under compressive fatigue loading.

Geometry nonlinearity of post buckling increases the numerical difficulties of a progressive delamination analysis. Zhang and Wang (2009a, b) simulated the delamination growth of a post-buckled laminate with pre-existing delamination under quasi-static compression by B-spline finite strip method. Hosseini-Toudeshky *et al*. (2010b) also developed a layer-wised finite element model to predict the delamination growth of post-buckled composite laminates under quasi-static compression loading using interface elements. Furthermore, Hosseini-Toudeshky *et al*. (2010c) investigated the effects of delamination size and stacking sequence of laminate on delamination growth under quasi-static compression loading by the layer-wised finite element modeling. However these large deformation simulations were performed under quasi-static loading and did performed under fatigue loading.

In this paper, delamination growths of post-buckled composite laminates under high cycle fatigue loading are analyzed. For this purpose, 20-node three-dimensional interface element with small thickness has been developed as a user element in ANSYS finite element software. As user material, mixed-mode bilinear constitutive law with consideration of damage growth under both cyclic loading and post buckling phenomena has been used in order to simulate the mixed-mode condition of stress field at large deformed delamination front. The finite element model considers the geometry nonlinearity of post-buckling and material nonlinearity of cohesive zone model. Various composite laminates under compressive cyclic loading are considered for the analyses and the obtained results are presented in this paper.

2. Element strain-displacement equations

In the finite element model of a laminate, interface elements connect any two adjacent layers via out of plane tangent and normal stresses. In the present finite element model, the laminate

undergoes post-buckling during delamination growth. Hence, large displacement strain-displacement equations should be considered for the laminate elements. Green equation of strain-displacement in tensor notation is

$$\varepsilon_{kl} = \frac{1}{2}\left(\frac{\partial U_k}{\partial X_l} + \frac{\partial U_l}{\partial X_k} + \frac{\partial U_m}{\partial X_k}\frac{\partial U_m}{\partial X_l}\right) \tag{1}$$

Where, U_1, U_2 and U_3 (or u, v and w) are displacements in the corresponding X_1, X_2 and X_3 (or x, y and z) directions. The product of $\frac{\partial U_m}{\partial X_k}\frac{\partial U_m}{\partial X_l}$ is the nonlinear term of strain. This term is considerable when multipliers are in order of magnitude larger than the linear terms. The dimension of laminates in the direction of Z is smaller than other two dimensions. So, the derivatives of the out of plane displacement (w) with respect to X and Y are considerably greater than other displacement derivatives under post-buckling or bending condition. Hence, the effective terms of large strain-displacement equations for a laminated element at an integration point are

$$\varepsilon_{xx} = \frac{\partial u}{\partial x} + \frac{1}{2}\left(\frac{\partial w}{\partial x}\right)^2 \tag{2}$$

$$\varepsilon_{yy} = \frac{\partial v}{\partial y} + \frac{1}{2}\left(\frac{\partial w}{\partial y}\right)^2 \tag{3}$$

$$\varepsilon_{zz} = \frac{\partial w}{\partial z} \tag{4}$$

$$\varepsilon_{xy} = \frac{1}{2}\left(\frac{\partial u}{\partial y} + \frac{\partial v}{\partial x} + \frac{\partial w}{\partial x}\frac{\partial w}{\partial y}\right) \tag{5}$$

$$\varepsilon_{yz} = \frac{1}{2}\left(\frac{\partial v}{\partial z} + \frac{\partial w}{\partial y} + \frac{\partial w}{\partial y}\frac{\partial w}{\partial z}\right) \tag{6}$$

$$\varepsilon_{xz} = \frac{1}{2}\left(\frac{\partial u}{\partial z} + \frac{\partial w}{\partial x} + \frac{\partial w}{\partial x}\frac{\partial w}{\partial z}\right) \tag{7}$$

On the other hand, the strain-displacement field for interface element contains of three components of out of plane shear and normal strains as illustrated in Fig. 1. Because of the nature of small thickness interface element, parallel slippage of vertical faces of interface element that form the thickness of element, (terms of $\partial w/\partial y$ and $\partial w/\partial x$ in Eqs. (6) and (7)) should not be contributed to produce the shear strains (ε_{xz} and ε_{yz}). On the other hand, the horizontal faces of interface lie on the laminate elements and the out of plane non-linear terms $\partial w/\partial y$ and $\partial w/\partial x$ in Eqs. (2), (3) and (5) produce large displacements in the interface element. So, the strain-displacement relations for shear strains at interface can be determined as follows

$$\varepsilon_{zz} = \frac{\partial w}{\partial z} \tag{8}$$

$$\varepsilon_{yz} = \frac{1}{2}\left(\frac{\partial v}{\partial z}\right) \tag{9}$$

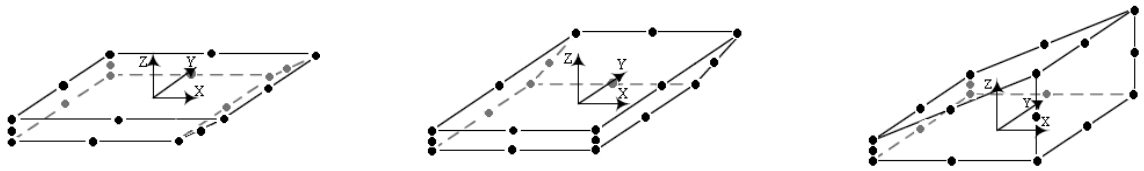

(a) $\varepsilon_{xz} = \frac{1}{2}(\frac{\partial u}{\partial z})$ (b) $\varepsilon_{yz} = \frac{1}{2}(\frac{\partial v}{\partial z})$ (c) $\varepsilon_{zz} = \frac{\partial w}{\partial z}$

Fig. 1 Components of interface element strains: (a) and (b) shear out of plane strains, (c) normal out of plane strain

$$\varepsilon_{xz} = \frac{1}{2}(\frac{\partial u}{\partial z}) \tag{10}$$

3. Interface constitutive law

A bilinear de-cohesive constitutive equation has been used in this article. The model follows the general formulation of solid-like interface element proposed by Balzani and Wagner (2008). The effective strain of an interface element under mixed-mode condition at an integration point has been determined by the following equations

$$\varepsilon_m = \sqrt{<\varepsilon_n>^2 + \gamma_{shear}^2} \ , \ \gamma_{shear} = \sqrt{\gamma_{sn}^2 + \gamma_{tn}^2} \tag{11}$$

Where the <> operator indicates the zero value for negative ε_n. The components of strain vector are as follows

$$\gamma_{sn} = 2\varepsilon_{yz} \tag{12}$$

$$\gamma_{tn} = 2\varepsilon_{xz} \tag{13}$$

$$\varepsilon_{sn} = \varepsilon_{zz} \tag{14}$$

The constitutive equation can be written as

$$\boldsymbol{\sigma} = \boldsymbol{D}\boldsymbol{\varepsilon} \tag{15}$$

Where $\boldsymbol{\varepsilon}$ and $\boldsymbol{\sigma}$ are interface strain and stress tensors and $\boldsymbol{D}$ is the elasticity tensor of interface which relates the interfacial stresses to the strains. It can be found as a function of damage parameter by the following equations

$$\boldsymbol{D} = \begin{cases} KI & \varepsilon_m \le \varepsilon_m^0 \\ (1-d)KI + dKI_c & \varepsilon_m^0 \le \varepsilon_m \le \varepsilon_m^f \\ KI_c & \varepsilon_m \ge \varepsilon_m^f \end{cases} \tag{16}$$

Where K is interface penalty stiffness and d is damage parameter. For zero-thickness interface elements, the penalty stiffness parameter is equal to the slope of the stress-relative displacement

curve. On the other hand for solid-like interface model, this parameter is the slope of stress-strain curve, so the stiffness of the solid-like element is 1/*t* times of the stiffness of the zero-thickness element and can be equal to the E_{33} value (Hosseini-Toudeshky *et al*. 2010b). ε_m^0 and ε_m^f are the effective strain at delamination onset and complete de-cohesion respectively, and

$$I_c = \begin{bmatrix} 0 & 0 & 0 \\ 0 & 0 & 0 \\ 0 & 0 & \dfrac{<\varepsilon_z>}{<-\varepsilon_z>} \end{bmatrix} \tag{17}$$

For bilinear constitutive equation, *d* can be determined by the following equation

$$d = \frac{\varepsilon_m^f(\alpha - \varepsilon_m^0)}{\alpha(\varepsilon_m^f - \varepsilon_m^0)} \tag{18}$$

Where α is the maximum applied ε_m in all previous iterations. Mode mixing ratio is also defined as

$$\beta = \frac{\gamma_{shear}}{\varepsilon_n} \tag{19}$$

To find the damage initiation stress, the following quadratic equation (Ye 1988) has been used

$$(\frac{<\sigma_n>}{\sigma_n^0})^2 + (\frac{\tau_{sn}}{\tau^0})^2 + (\frac{\tau_{tn}}{\tau^0})^2 - 1 = 0 \tag{20}$$

In this equation σ_n^0 and τ^0 are normal and shear interfacial strengths. Using Eqs. (1), (4) and (5), the effective strain at the delamination onset, ε_m^0, can be found as follows

$$\varepsilon_m^0 = \begin{cases} \varepsilon_n^0 \gamma^0 \sqrt{\dfrac{1+\beta^2}{(\gamma^0)^2 + (\beta\varepsilon_n^0)^2}} & \varepsilon_n > 0 \\ \gamma^0 & \varepsilon_n \le 0 \end{cases} \tag{21}$$

The B-K (Benzeggagh and Kenane 1996) relation has been used to determine critical energy release rate (G_c) and energy release rate threshold (G_{th}) in mixed-mode fracture condition. It has been assumed that the critical energy release rate per thickness of interface is equal to the area under effective stress-strain relation. By this assumption, the effective strain at complete de-cohesion is

$$\varepsilon_m^f = \begin{cases} \dfrac{2}{Kh_0\varepsilon_m^0}(G_{IC} + (G_{IIC} - G_{IC})(\dfrac{G_T - G_I}{G_T})^\eta) & \varepsilon_n > 0 \\ \gamma_{sn}^f & \varepsilon_n \le 0 \end{cases} \tag{22}$$

Where h_0 is the interface element thickness and η is a material parameter obtained from experiments. G_T is the sum of pure modes of energy release rate.

Fatigue crack growth can be considered as a summation of the damage created by quasi-static overloads and the damage created by cyclic loads (Turon *et al*. 2007a)

$$d = d_{static} + d_{cyclic} \tag{23}$$

The evolution of damage parameter created by cyclic loading can be found from (Turon *et al*. 2007a)

$$\frac{\partial d}{\partial N} = \frac{\partial d}{\partial A_d}\frac{\partial A_d}{\partial N} \tag{24}$$

Where, A_d is damaged area of element. It can be derived from Eq. (18) that

$$\frac{\partial d}{\partial A_d} = \frac{1}{A_e}\frac{(\varepsilon_m^f(1-d)+d\varepsilon_m^0)^2}{(\varepsilon_m^f\varepsilon_m^0)} \tag{25}$$

Where, A_e is element area. By assuming A_{CZ} as the cohesive zone area, it can be written that (Turon *et al*. 2007a)

$$\frac{\partial A_d}{\partial N} = \frac{A_e}{A_{CZ}}\frac{\partial A}{\partial N} \tag{26}$$

Where, $\frac{\partial A}{\partial N}$ is crack growth rate. A_{cz} is estimated using Rice closed-form equation (Rice 1979, Turon *et al*. 2007b)

$$A_{CZ} = b\frac{9\pi}{32}\frac{E_3 G^{\max}}{\tau_0^2} \tag{27}$$

Where G^{max} varies from G_{IC} to G_{IIC} as ε_m varies from ε_m^0 and ε_m^f. Since in this paper the load ratio in the fatigue cycles are zero, the G^{max} value is equal to ΔG and can be calculated by Eq. (29). The required sufficient number of interface elements along the length of cohesive zone is not well established. Falk *et al*. (2001) used between 2 and 5 elements in the length of cohesive zone. Mi *et al*. (1998) also suggested the use of at least 2 elements in the cohesive zone length. Therefore, according to the recommendations of previously performed investigations, 5 elements can be used along the cohesive zone length to predict the delamination growth.

Paris Law has been also used to calculate the fatigue crack growth rate

$$\frac{\partial A}{\partial N} = \begin{cases} C(\frac{\Delta G}{G_C})^m & G^{\max} > G_{th} \\ 0 & G^{\max} \le G_{th} \end{cases} \tag{28}$$

Where, ΔG is the area under effective stress-strain curve at current effective strain as follows

$$\Delta G = \frac{h_0\varepsilon_m^0 K}{2}(\varepsilon_m^f - \frac{(\varepsilon_m^f - \varepsilon_m)^2}{(\varepsilon_m^f - \varepsilon_m^0)}) \tag{29}$$

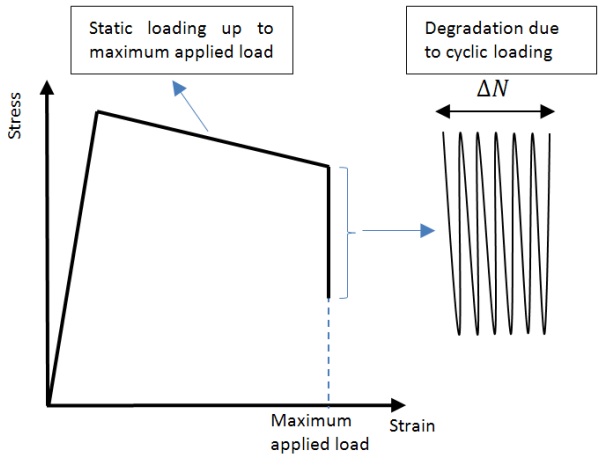

Fig. 2 Constitutive law of bilinear interface element under applied static and cyclic loading.

The mode dependency of C and m are considered by the following equations (Blanco *et al.* 2005)

$$\log C = \log C_I + (\frac{G_{II}}{G_T}) \log C_m + (\frac{G_{II}}{G_T})^2 \log \frac{C_{II}}{C_I C_m} \tag{30}$$

$$m = m_I + (\frac{G_{II}}{G_T}) m_m + (\frac{G_{II}}{G_T})^2 (m_{II} - m_I - m_m) \tag{31}$$

Where, G_I and G_{II} are pure mode I and II energy release rates. C_I, C_{II}, m_I and m_{II} are pure mode I and II crack growth rate parameters. C_m and m_m are the mode-ratio material parameters that must be determined by curve-fitting experimental data.

The constitutive law for interface element considering the static and cyclic loading is illustrated in the Fig. 2. The cycle jump strategy has been used here to skip ΔN cycles in each step. After calculating $\partial d^P_i/\partial N$ using Eq. (24), the damage evolution has been simulated at the integration point, P, within the element by the following equation

$$d^P_{i+\Delta N} = d^P_i + (\frac{\partial d^P_i}{\partial N}) \Delta N \tag{32}$$

4. Results and eiscussion

The presented interface element and user material has been linked to ANSYS software by user programmable features. The interface element is a three-dimensional 20-node brick element with small thickness. A very thin initial thickness of interface – e.g., about 1/100 of the laminate thickness – is sufficient to neglect the effect of bending moments which might be produced by the eccentricities of the nodal forces (Wagner and Balzani 2008). To verify the user element and user material subroutine, a single element size model and an available delamination growth model have been analyzed by the developed procedure.

Table 1 Material properties for HTA/6376C graphite/epoxy

E_{11} (GPa)	E_{22}=E_{33} (GPa)	G_{12}=G_{13} (GPa)	G_{23} (GPa)	$\nu_{12}=\nu_{13}$	ν_{13}
120	10.5	5.25	3.48	0.3	0.41
G_{Ic} (N/mm)	G_{IIc} (N/mm)	G_{IIIc} (N/mm)	σ_o (MPa)	τ_0 (MPa)	η
0.26	1.002	1.002	30	30	2.73
m_I	C_I (mm/cycle)	m_{II}	C_{II} (mm/cycle)	m_m	C_m (mm/cycle)
5.09	2.1	4.5	2.99	4.94	458087

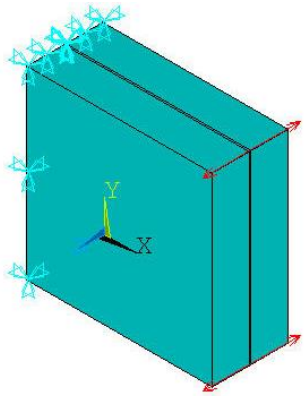

Fig. 3 Single element size model

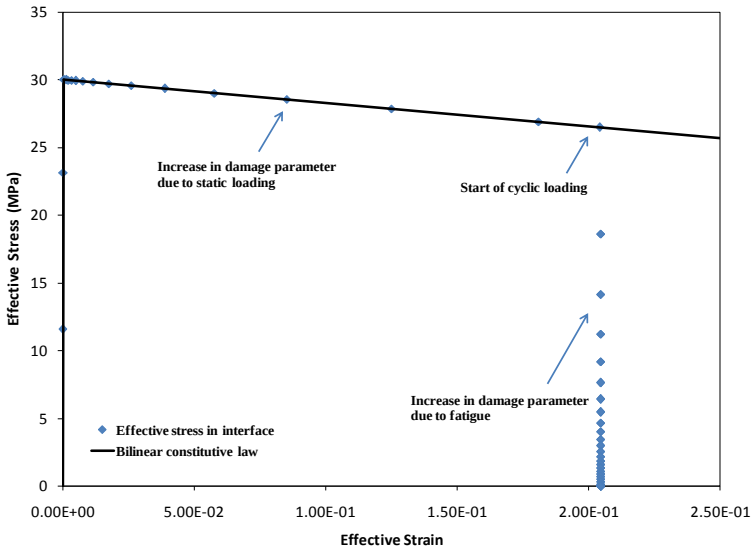

Fig. 4 Effective stress versus effective strain at interface in a single element size model

4.1 Single element size model

In this model, an interface element considered between two laminated elements subjected to cyclic normal tension loading. Each laminated element is a zero angle lamina of carbon-epoxy

HTA/6376C with material properties listed in Table 1 (Asp *et al*. 2001, Juntti *et al*. 1999, Robinson *et al*. 2005) with 0.2 mm thickness and 1 mm length and width. G_{IIIc} has been assumed to be equals to G_{IIc}. The thickness of interface element is 0.01 mm and the interface penalty stiffness is 10 GPa. The geometry and applied loads of the model are presented in Fig. 3.

The displacement type loading was applied with the maximum value of 0.002 mm at the end of each 1000 cycles. Fig. 4 shows the obtained effective stress versus effective strain at interface in the location of applied load. This figure shows an excellent agreement between the obtained results and bilinear constitutive law data up to the maximum achieved applied load. After that, fatigue loading gradually degrades the stiffness of interface and vanishes to zero value.

4.2 Delamination growth model

For more validation of the developed procedure, the obtained results of a composite laminate with initial delamination under quasi-static compressive loading are compared with the available numerical results in Zhang and Wang (2009b). The model has 50.8 mm length and 5.08 mm width. Layup configuration is $[0_4//0_{12}/0_4]$ in which the // sign is the place of pre-existed delamination with initial length of 38.1 mm. The thickness of interface element equals to 0.01 mm. The penalty stiffness is 10 GPa. An imperfection has been applied to the model with maximum value of 0.01 mm at the middle of 4-layer upper and 16-layer lower laminate in opposite directions. Thickness of each layer is 0.129 mm and the material of laminate is T300/976 graphite/epoxy, the properties of which are presented in Table 2 (Zhang and Wang 2009b).

The obtained variation of applied load versus central deflection of the model has been illustrated in Fig. 5. To investigate the effect of mesh size on the results, the model has been analyzed with two different mesh sizes. Two models with coarse mesh containing of 420 elements and the fine mesh contains of 750 elements were analyses. This figure shows a reasonable agreement between the results of finite strip method (Zhang and Wang 2009b) and present study. The obtained global buckling load for the present model is 1.5% smaller than that from the finite strip method. Fig. 5 also shows very well agreement between the obtained results with coarse and fine mesh models.

4.3 Compressive fatigue delamination growth

To evaluate the delamination growth in a laminate containing initial delamination under compressive fatigue loading, laminates with the material properties of HTA/6376C (graphite/epoxy) presented in Table 1 (Asp *et al*. 2001, Juntti *et al*. 1999, Robinson *et al*. 2005) have been analysed using the developed approach. Again, the thickness of interface element is 0.01 mm. The interface penalty stiffness has been taken to be 10 GPa. Two laminates have been analyzed using the present approach to observe the effect of the dept of initial delamination on the delaminatin growth rate. The lay-up configurations in these two laminates are $[0_4//0_4/0_4]$ and

Table 2 Material properties for T300/976 graphite/epoxy

E_{11} (GPa)	E_{22}=E$_{33}$ (GPa)	G_{12}=G_{13} (GPa)	G_{23} (GPa)	$\nu_{12}=\nu_{13}$	ν_{13}
139.3	9.72	5.58	3.45	0.29	0.4
G_{Ic} (N/mm)	G_{IIc} (N/mm)	G_{IIIc} (N/mm)	η	σ_o (MPa)	τ_0 (MPa)
0.0876	0.3152	0.3152	2.68	44.54	106.9

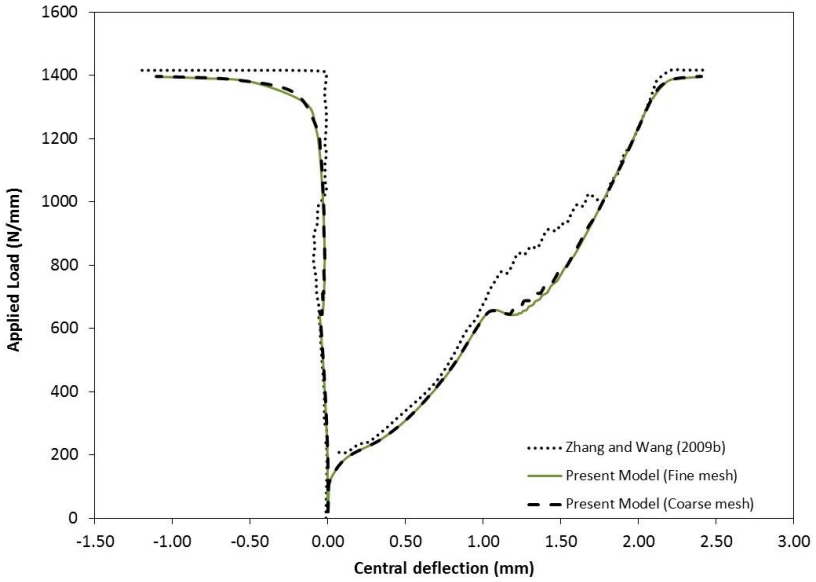

Fig. 5 Comparison of the obtained applied Load versus central deflection from this study with Zhang and Wang (2009b) for $[0_4//0_{12}/0_4]$ laminate

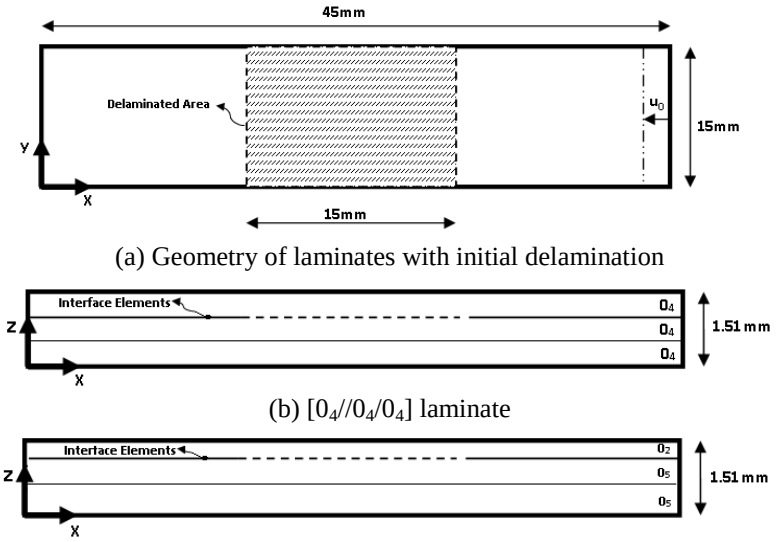

(a) Geometry of laminates with initial delamination

(b) $[0_4//0_4/0_4]$ laminate

(c) $[0_2//0_5/0_5]$ laminate

Fig. 6 Geometry of laminate

$[0_2//0_5/0_5]$. Thickness of each layer is 0.125 mm. The geometry of the laminates are illustrated in Fig. 6. In these models, 90 elements were used along the length and 5 elements along the width. For the upper sub-laminates ($[0_4]$ and $[0_2]$), the models contain of 1 element along the sub-laminate thickness. For the lower sub-laminates ($[0_4/0_4]$ and $[0_5/0_5]$), the models contain of 2 elements in the sub-laminate thickness. Totally, each model contains of 1650 elements where 300 elements of

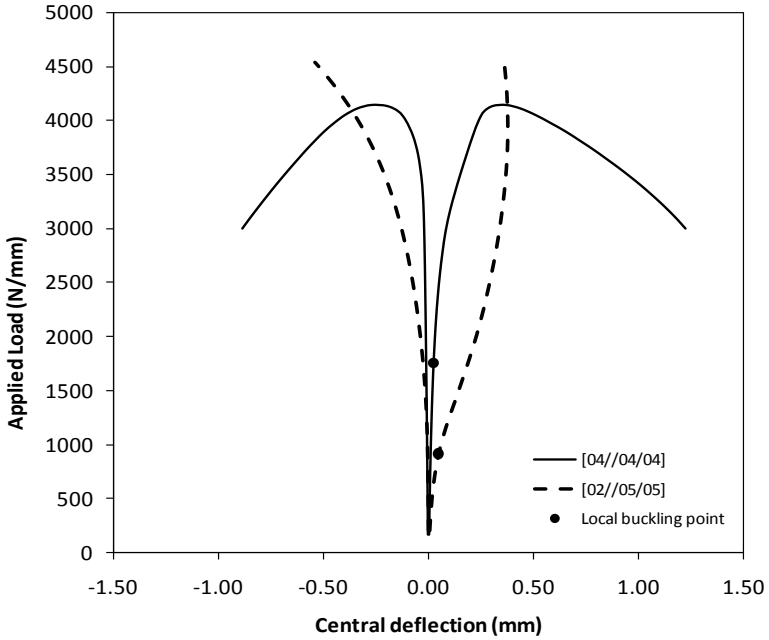

Fig. 7 Applied load versus central out of plane deflection for different laminates

them are interface elements with the length of 0.5 mm for each element. According to equation (27), the minimum area of cohesive zone area for the models in mode one is 40.20 mm^2. So the minimum length of the cohesive zone (A_{CZ}/b) is 2.68 mm. Therefore with the length of 0.5 mm for the interface elements, the cohesive zone contains of at least 5 elements. An imperfection of 0.03 mm is applied to the middle of laminates on nodes at x = 22.5 mm and z = 1.5 mm for upper sub-laminate and -0.03 mm on nodes at x = 22.5 mm and z = 0 mm for lower sub-laminate. End shortening of 0.135 mm have been applied to the end of laminates.

The diagram of applied load versus deflection of middle point of the $[0_2//0_5/0_5]$ and $[0_4//0_4/0_4]$ laminates after static loading are presented in Fig. 7. In the $[0_2//0_5/0_5]$ laminate, the $[0_2]$ sub-laminate moves backward after the global buckling of $[0_5/0_5]$ laminate. According to Fig. 7, the local buckling load of the $[0_4//0_4/0_4]$ laminate is 1754 N and $[0_2//0_5/0_5]$ laminate is 913 N. The local buckling of laminate has been considered to occur when the amount of incremental applied force at the end of laminate is reduced.

Then the cyclic loading started with the maximum displacement value of 0.135 mm. The R-ratio of cyclic loading is zero. The contours of damage parameter at interfaces showing the delamination growth were obtained for both laminates, at several intervals up to100000 cycles and depicted in Fig. 8. The damage parameter value of 1 in an integration point of an element means debonding at that integration point. This figure shows that the laminate with deeper initial delamination from the free surface (the $[0_4//0_4/0_4]$ laminate), prone to a large delamination growth under post buckling static loading and the faster delamination growth under cyclic loading.

The deformed shapes of laminates containing the information of mixed mode buckling and delamination growth after static loading and 100000 cyclic loading have been presented in Fig. 9. This figure shows considerable delamination growth after 100000 compression cyclic loading for both laminates.

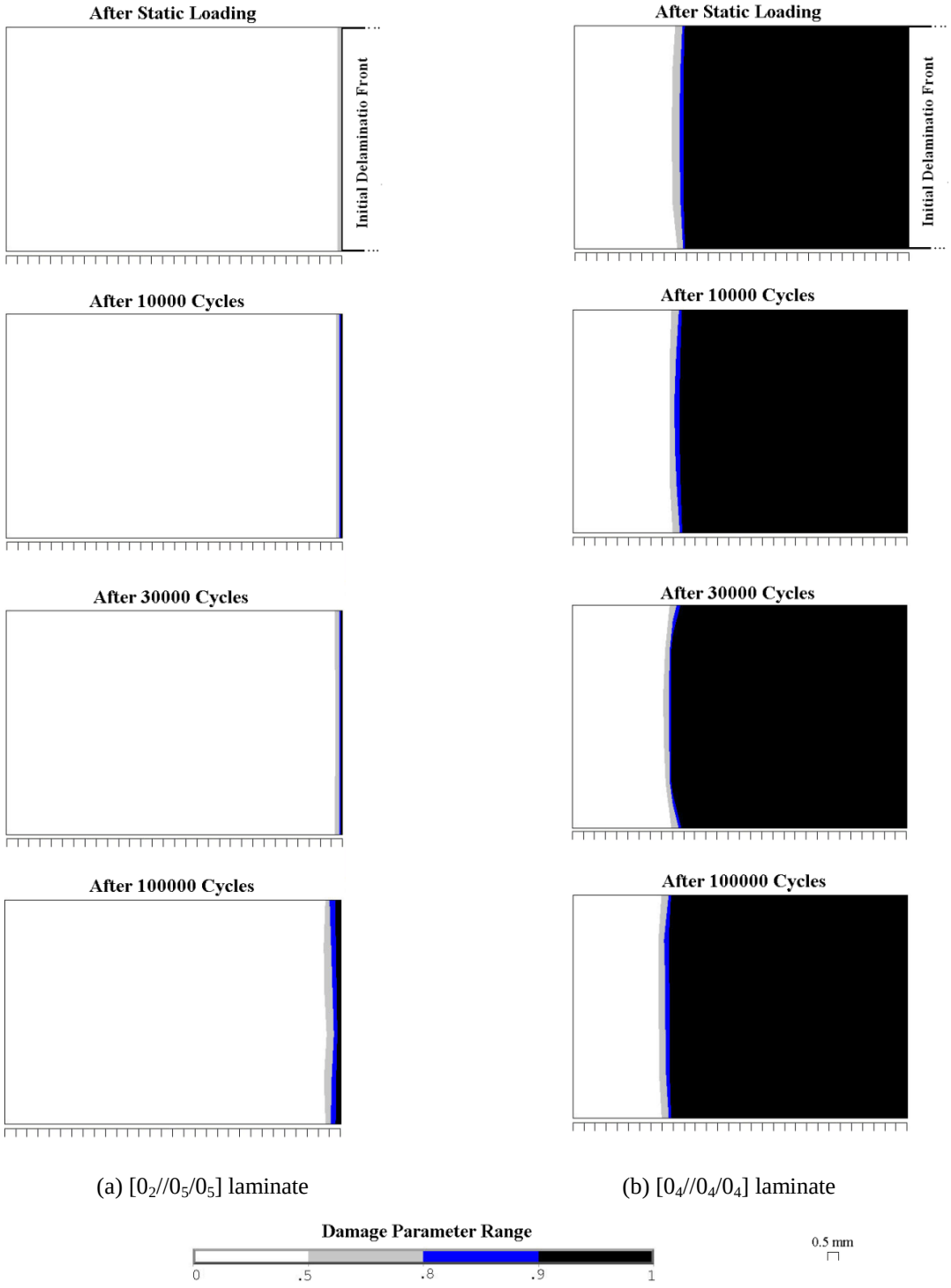

(a) $[0_2//0_5/0_5]$ laminate (b) $[0_4//0_4/0_4]$ laminate

Fig. 8 Contour of damage parameter under static and compressive fatigue loading at interface with initial delamination: (a) $[0_2//0_5/0_5]$ laminate and (b) $[0_4//0_4/0_4]$ laminate

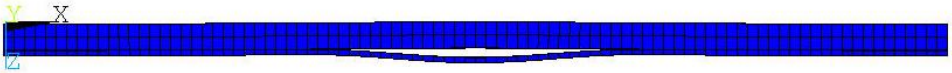

(a) $[0_2//0_5/0_5]$ laminate after static loading

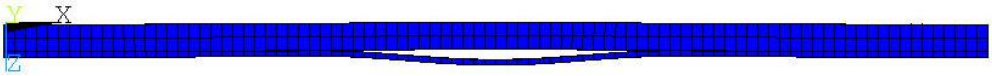

(b) $[0_2//0_5/0_5]$ laminate after 100000 cyclic loading

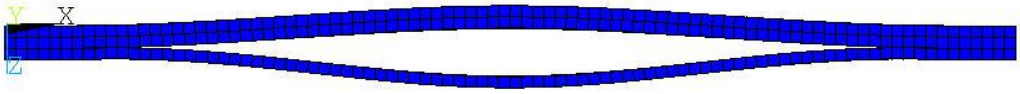

(c) $[0_4//0_4/0_4]$ laminate after static loading

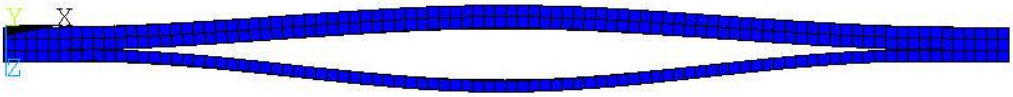

(d) $[0_4//0_4/0_4]$ laminate after 100000 cyclic loading

Fig. 9 Deformed shape of laminates under post buckling

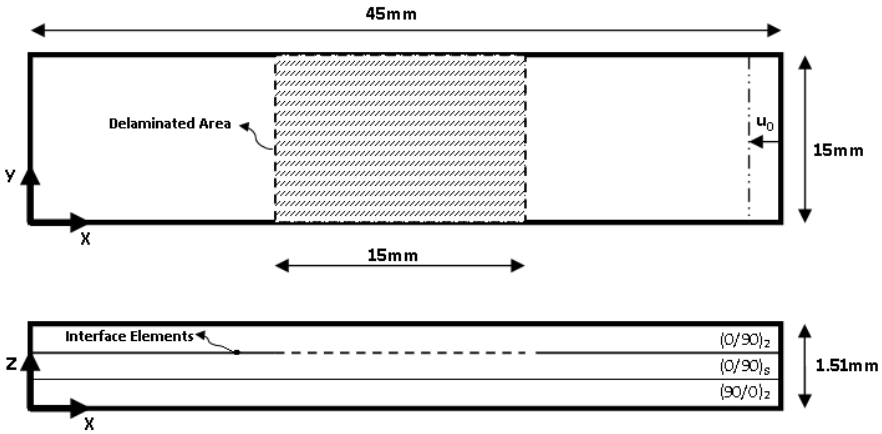

Fig. 10 Geometry of the cross-ply laminate,$[(0/90)_2//(0/90)_s/(90/0)_2]$

Furthermore, a laminate with cross-ply layup configuration is analysed using the present approach. The obtained results of cross-ply laminates with lay-up configuration of $[(0/90)_2//(0/90)_s/(90/0)_2]$ are compared with those from the unidirectional layup of $[0_4//0_4/0_4]$.The geometry of cross-ply laminate is illustrated in Fig. 10, while the laminate with unidirectional layup discussed above in the previous example. The number of elements in the length, width and thickness direction are similar to the previous example. An Imperfection has also been applied to the model similar to the previous example.

End shortening of 0.135 mm have been applied to the end of laminate. Variations of the obtained applied load versus deflection of middle point of cross-ply laminate have been presented in Fig. 11. The local buckling load of this laminate is 717 N.

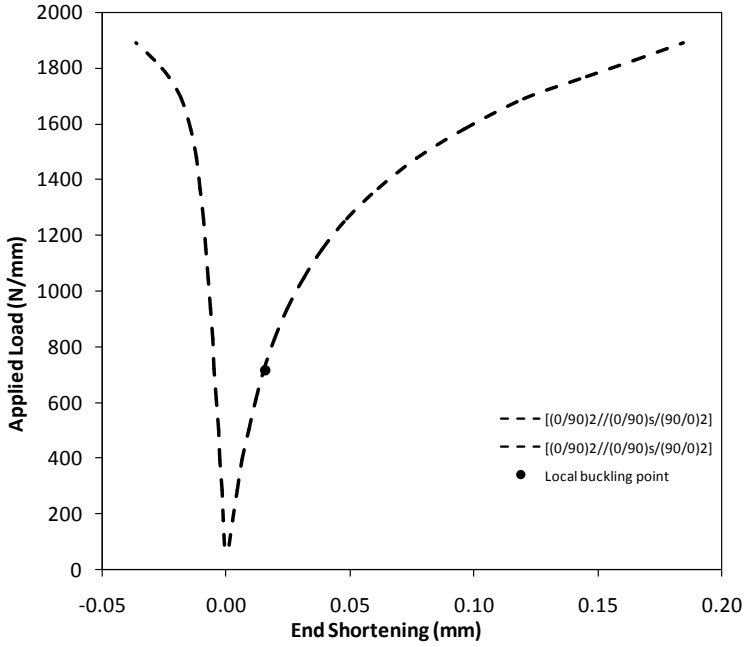

Fig. 11 Applied load versus central out of plane deflection for $[(0/90)_2//(0/90)_s/(90/0)_2]$ laminate

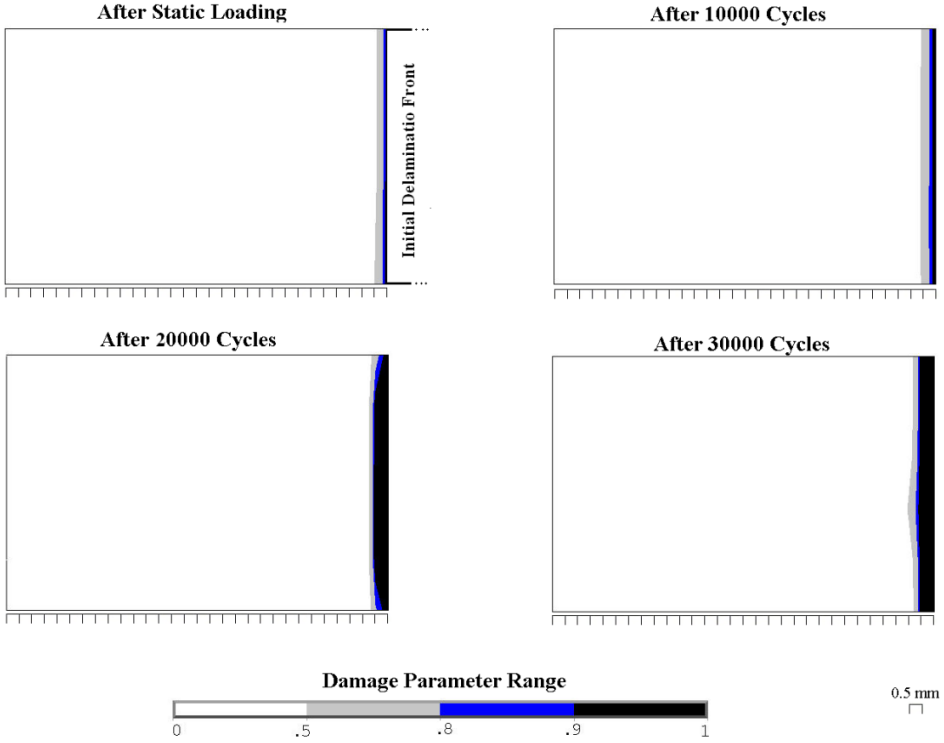

Fig. 12 Contour of damage parameter under compressive fatigue loading at interface elements of $[(0/90)_2//(0/90)_s/(90/0)_2]$ laminate

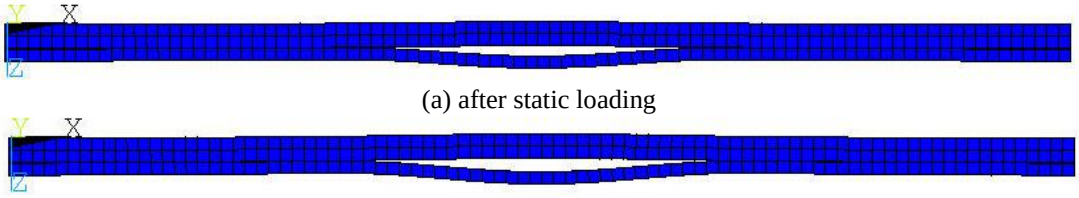

(a) after static loading

(b) after 30000 cycles

Fig. 13 Deformed shape of $[(0/90)_2//(0/90)_s/(90/0)_2]$ laminate under post buckling

The maximum value of applied displacement at cyclic loading for the $[(0/90)_2//(0/90)_s/(90/0)_2]$ laminate is 0.135 mm. The load ratio of cyclic loading is also zero. The obtained contours of damage parameter at interface, ahead of delaminated area of laminate after 30000 cycles have been presented in Fig. 12.

It can be observed from Figs. 8 and 12 that delamination in the unidirectional $[0_4//0_4/0_4]$ laminate growth faster than the cross-ply $[(0/90)_2//(0/90)_s/(90/0)_2]$ laminate. The deformed shape of $[(0/90)_2//(0/90)_s/(90/0)_2]$ laminate with the applied end shortening of 0.135 mm have been illustrated in Fig. 13 showing considerable delamination growth after 30000 compression load cycles.

5. Conclusions

A three-dimensional interface element with mixed-mode bilinear constitutive law has been presented in this paper for prediction of delamination growth of laminates under compressive cyclic loading with geometry nonlinearity behavior. To verify the developed procedure, the predicted load deflection diagram for a composite laminate with initial delamination has been compared with the available data from the literature. Moreover, delamination growths of two composite laminates under cyclic pressure loadings were investigated. It was shown that the laminate with closer initial delamination to the middle of laminate prone to more delamination growth. It was also shown that the delamination growth in cross-ply laminate is smaller than the unidirectional laminate under similar cyclic loading condition.

References

Asp, L., Sjoogren, A. and Greenhalgh, E. (2001), "Delamination growth and thresholds in a carbon/epoxy composite under fatigue loading", *J. Compos. Techol. Res.*, **23**, 55-68.

Benzeggagh, M. and Kenane, M. (1996), "Measurement of mixed-mode delamination fracture toughness of unidirectional glass/epoxy composites with mixed-mode bending apparatus", *J. Compos. Sci. Techol.*, **56**, 439-49.

Blanco, N., Gamstedt, E., Asp, L. and Costa, J. (2005), "Mixed-mode delamination growth in carbon–fibre composite laminates under cyclic loading", *Int. J. Solids. Struct.*, **41**, 4219-4235.

Camanho, P. and Davila, C. (2002), "Mixed-mode de-cohesion finite elements for the simulation of delamination in composite materials", NASA Report-No. TM-2002-211737.

Falk, M., Needleman, A. and Rice, J. (2001), "A critical evaluation of cohesive zone models of dynamic fracture", *J. de Physique IV, Proceedings*, 543-550.

Griffith, A. (1921), "The phenomena of rupture and flow in solids", *Philosophical Transactions of the Royal Society of London*, **221**, 163-198.

Hosseini-Toudeshky, H., Hosseini, S. and Mohammadi, B. (2010a), "Progressive delamination growth analysis using discontinuous layered element", *J. Compos. Struct.*, **92**, 883-890.

Hosseini-Toudeshky, H., Hosseini, S. and Mohammadi, B. (2010b), "Delamination buckling growth in laminated composites using layer-wise interface element", *J. Compos. Struct.* , **92**, 1846-1856.

Hosseini-Toudeshky, H., Hosseini, S. and Mohammadi, B. (2010c), "Buckling and Delamination Growth Analysis of Composite Laminates Containing Embedded Delaminations", *Appl. Compos. Mater.*, **17**, 95-109.

Hosseini-Toudeshky, H., Jasemzadeh, A. and Mohammadi, B. (2011), "FatigueDebonding Analysis of Repaired Aluminium Panels by Composite Patch using Interface Elements", *Appl. Compos. Mater.*, **18**, 571-584.

Juntti, M., Asp, L. and Olsson, R. (1999), "Assessment of evaluation methods for the mixed-mode bending test", *J. Comp. Technol. Res.*, **21**, 37-48.

Kardomateas, G., Pelegry, A. and Malik, A. (1995), "Growth of Internal Delamination under Cyclic Compression in Composite Plates", *J. Mech. Phys. Solids*, **43**(6), 847-868.

Krueger, R. (2002), "The virtual crack closure technique: history, approach and applications", NASA CR-2002-211628.

Mi, U., Crisfield, M. and Davies, G. (1998), "Progressive delamination using interface elements", *J. Compos. Mater.*, **32**, 1246-1272.

Rice, J.R., Dziewonski, A.M. and Boschi, E. (1980), P"hysics of the Earth's Interior, the mechanics of earthquake rupture", *Proceedings of the International School of Physics, Italian Physical Society, Course LXXVIII*, Varenna, Italy.

Robinson, P., Galvanetto, U., Tumino, D. and Bellucci, G. (2005), "Numerical Simulation of Fatigue-driven Delamination using Interface Elements", *Int. J. Numer. Meth. Eng.*, **63**, 1824-1848.

Rybicki, E. and Kanninen, M. (1977), "A finite element calculation of stress intensity factors by a modified crack closure integral", *J. Eng. Fract. Mech.*, **9**,931-938.

Turon, A., Costa, J., Camanho, P. and Davila, C. (2007a), "Simulation of delamination in composites under high-cycle fatigue", *Compo. Part A: Appl. Sci. Manuf.*, **38**(11), 2270-2282.

Turon, A., Davila, C., Camanho, P. and Costa, J. (2007b), "An engineering solution for solving mesh size effects in the simulation of delamination with cohesive zone models", *J. Eng. Fract. Mech.*, **74**(10), 1665-1682.

Wagner, W. and Balzani, C. (2008), "An Interface Element for the Simulation of Delamination in Unidirectional Fiber-reinforced Composite Laminates", *J Eng. Fract. Mech.*, **75**, 2597-2615.

Ye, L. (1988), "Role of matrix resin in delamination onset and growth in composite laminates", *J. Compos Sci. Technol.*, **33**, 257-277.

Zhang, Y. and Wang, S. (2009a), "Buckling, post-buckling and delamination propagation in debonded composite laminates part1: theoretical development", *J. Compos. Struct.*, **88**, 121-130.

Zhang, Y. and Wang, S. (2009b), "Buckling post-buckling and delamination propagation in debonded composite laminates part2: numerical application", *J. Compos. Struct.*, **88**, 131-146.